Thickness evaluation of AlO_x barrier layers for encapsulation of flexible PV modules in industrial environments by normal reflectance and machine learning

Enric Grau-Luque,[1] Maxim Guc,[1] Ignacio Becerril-Romero*,[1] Alejandro Pérez-Rodríguez,[1,5] Pieter Bolt,[2] Fieke van den Bruele,[3] Ulfert Ruhle[4] and Víctor Izquierdo-Roca*[1]

[1]*Catalonia Institute for Energy Research (IREC), Jardins de les Dones de Negre 1, 08930 Sant Adrià del Besòs (Barcelona), Spain*

[2]*TNO, Department of Solar Technology and Applications, High Tech Campus 21, 5656 AE Eindhoven, The Netherlands*

[3]*TNO, Holst Centre, High Tech Campus 31, 5656 AE Eindhoven, The Netherlands*

[4]*FLISOM AG, Gewerbestrasse 16, 8155 Niederhasli, Switserland*

[5]*IN²UB, Departament Enginyeria Electrònica i Biomèdica, Universitat de Barcelona, c. Martí i Franquès 1, 08028 Barcelona, Spain*

**E-mail: ibecerril@irec.cat, vizquierdo@irec.cat*

Abstract

Flexible photovoltaic (PV) devices, such as those based on CIGS and perovskites, use polymeric front sheets for encapsulation that do not provide sufficient protection against the environment. The addition of nanometric Al_xO layers by spatial atomic layer deposition (S-ALD) to these polymeric materials can highly improve environmental protection due to their low water vapor transmission rate and is a suitable solution to be applied in roll-to-roll industrial production lines. A precise control of the thickness of the AlO_x layers is crucial to ensure an effective water barrier performance. However, current thickness evaluation methods of such nanometric layers are costly and complex to incorporate in industrial environments. In this context, the present work describes and demonstrates a novel characterization methodology based on normal reflectance measurements and either on control parameter-based calibration curves or machine learning algorithms that enables a precise, low-cost and scalable assessment of the thickness of AlO_x nanometric layers. In particular, the proposed methodology is applied

for precisely determining the thickness AlO_x nanolayers deposited on three different substrates relevant for the PV industry: monocrystalline Si, $Cu(In,Ga)Se_2$ multi-stack flexible modules and polyethylene terephthalate (PET) flexible encapsulation foil. The proposed methodology demonstrates a sensitivity < 10 nm and acquisition times ≤ 100 ms which makes it compatible with industrial monitoring applications. Additionally, a specific design for in-line integration of a normal reflectance system into a roll-to-roll production line for thickness control of nanometric layers is defined and proposed.

Keywords: flexible PV, encapsulation, AlO_x, normal reflectance, process monitoring, CIGS, machine learning, thickness assessment

1. Introduction

Light weight and flexible photovoltaic (PV) modules fully exploit the technological capabilities of thin film photovoltaics since, besides their inherent advantages such as reduced fragility and adaptation to curved surfaces that open the way to numerous applications, they can be fabricated through high throughput roll-to-roll (RtR) processes. This type of intensive production reduces both the economic and energy costs of PV, leading to devices with an increased energy return on energy invested (EROI) ratio, key for the expansion of solar energy.[1] A critical step in the fabrication of flexible PV modules is the implementation of a suitable encapsulation architecture. Contrarily to the standard rigid modules that typically employ glass sheets for this purpose, the encapsulation of flexible photovoltaic modules, like those based on e.g. $Cu(In,Ga)Se_2$ (CIGS) or perovskite absorber materials, relies on the use of flexible transparent polymeric front sheets.[2] These commonly present reduced water vapour barrier properties and require additional protective layers to ensure a proper environmental protection and long term preservation of the modules.[2,3] In this regard, AlO_x-based nanolayers deposited on the polymeric front sheets by atomic layer deposition (ALD) have been demonstrated to possess a high conformity and compactness which confer them a very low water vapour transmission rate.[4–9] However, conventional ALD is an extremely slow deposition technique (200 mm/h in RtR configuration to achieve 25 – 30 nm thick layer)[4] incompatible with industrial high throughput processing. On the other hand, spatial ALD (S-ALD) is a technological alternative to standard ALD in which, in simple terms, the samples move between spatially-separated half-reaction zones where the deposition takes place. As a consequence, the deposition rate is mainly limited by the amount of deposition areas and the time required to move the samples between them achieving deposition rates ~1 nm/s which are fully compatible with RtR web speeds.[10,11]

In the case of CIGS, on which this work is focused, it has also been demonstrated that, in addition to the employment of AlO_x-deposited polymeric front sheets, AlO_x nanolayers can also be directly applied on the top electrode of the devices and still provide high end barrier properties.[5] In this context, S-ALD-deposited AlO_x barriers break ground to low cost and RtR-compatible front sheet solutions that represent a step forward for the production flexible PV devices. Furthermore, the use of AlO_x nanolayers in PV is not limited to encapsulation and AlO_x layers have also been successfully employed for interface engineering and passivation in thin films solar cells and other devices [12–16].

Like with most applications in which nanocoatings are employed, a precise thickness control of the applied AlO_x nanolayers is crucial for them to function properly and provide the desired effect. In the case of flexible PV module encapsulation, the water vapour barrier properties of AlO_x nanolayers have been reported to drop dramatically when their thickness falls below 10 nm[8] while their brittleness increases with layer thickness making it more prone to fracture under bending stresses on flexible substrates.[17] As such, a precise thickness control is required to ensure an adequate functionality of the AlO_x layers for their use as water vapor barriers in flexible PV devices. Likewise, precise thickness control is also critical for other uses of AlO_x layers like interface passivation[18]. In this context, the development of methodologies and tools that can be implemented at RtR lines for in-line process monitoring represents a strategic technological advance for improving and optimizing PV module production at mass scale.

The reduced thickness of nanocoatings commonly requires the use of very specific characterization techniques like those based on X-ray photoelectron spectroscopy,[19,20] atomic force and electron microscopy,[21,22] Rutherford backscattering spectroscopy,[23] ellipsometry[4,13,15,16,18,24–26] or transmittance-reflectance spectroscopy,[8,27,28] among others. These techniques either require long acquisition times, sample destruction, and/or high energy (deep UV or X-ray) excitation wavelengths. Moreover, some of the mentioned techniques suffer from limitations related to the characteristics of the nanocoated substrate (high roughness and/or multi-stack configuration, sensitivity to high excitation energies etc.) and/or cannot be applied to large area analyses. All these issues make the implementation of the existing methods in high-throughput production lines very technically challenging and economically costly.

Another critical issue regarding the scaling up of the production of flexible PV devices is layer homogeneity. In fact, homogeneity is usually considered one the most important barriers for the transference of CIGS PV devices from the laboratory to the industry level.[29] In this regard,

the implementation of techniques that allow performing fast large-area mappings to monitor layer homogeneity is also of great relevance for the industry.

In this framework, this work describes and demonstrates a novel non-destructive, fast, precise, low-cost and scalable characterization method for determining the thickness of AlO_x nanometric layers (from a few to around 100 nm) that is compatible with both research and industrial process monitoring environments. This approach is based on normal reflectance measurements and takes advantage of the impact of quantum confinement (QC) effects on the optical properties of AlO_x nanolayers as a consequence of their nanometric thickness: optical bandgap (E_g) and optical constants (n and k).[30] The viability and effectiveness of the technique are demonstrated for precisely determining the thickness of AlO_x nanometric layers deposited by S-ALD on different relevant materials for the PV industry with different characteristics: monocrystalline Si wafers (smooth), a complete CIGS module (multi-stack substrate), and polyethylene terephthalate (PET) polymer encapsulating sheets (rough). We demonstrate that the slight QC-induced changes in the optical properties of the AlO_x layers can be detected from normal reflectance measurements with a simple setup and be used for layer thickness determination with resolutions better than 10 nm through their combination with machine learning algorithms. The compatibility of the proposed approach with fast micro (tenths of microns) and macro (up to several m^2) mapping analyses, depending on the application, as well as the possibility of modifying the system employed, for better compatibility with in-line industrial process monitoring, are analysed and discussed.

2. Experimental

Data acquisition and sample description

Figure 1 shows the normal reflectance probe that was implemented in this work and used for the evaluation of the thickness of AlO_x nanolayers with a broad emission (400 – 1000 nm, approximately) halogen lamp as illumination source. The probe was coupled to an XY-crane to enable mapping measurements and the acquired signal was processed through a compact CCD spectrometer (Thorlabs CCS200). A vacuum chuck table was employed to ensure the flatness of flexible samples during measuring. A spot size of ~100 µm and acquisition times in the 10-100 ms range (depending on the type of sample analysed) were employed for the measurements.

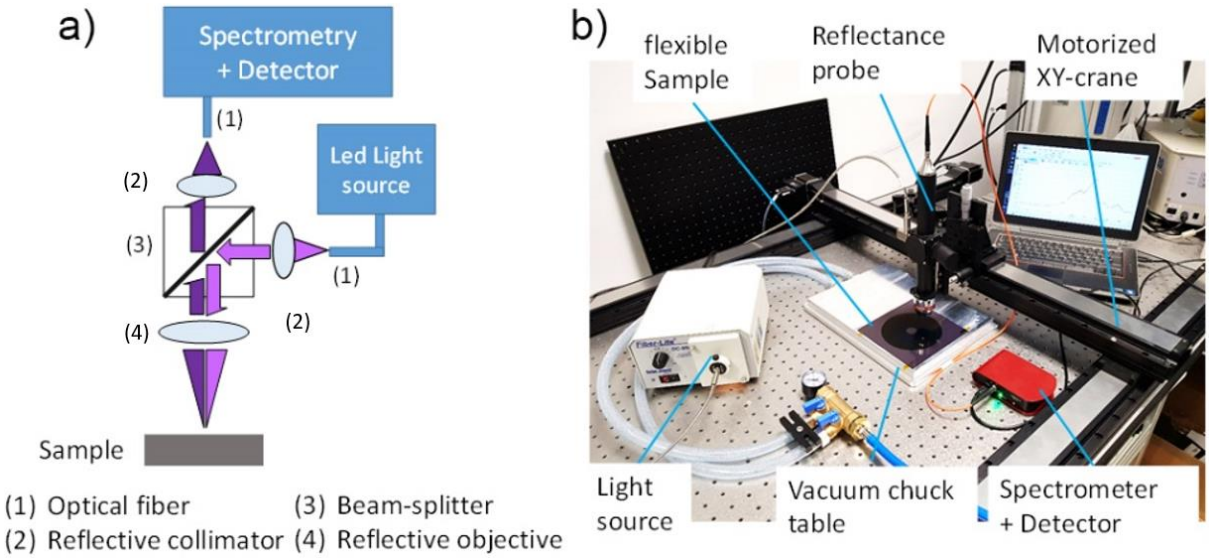

Figure 1. a) Schematic of the normal reflectance probe based in a broad emission halogen lamp and b) picture of the implemented system.

The system described above was employed on different sets of samples for the evaluation of the thickness of nanometric AlO_x layers deposited by means of a laboratory-scale rotary spatial-ALD reactor[31] on relevant substrates for the PV industry: i) three monocrystalline Si substrates coated with 25, 50 and 75 nm AlO_x layers, ii) six 15×15 cm^2 complete (non-encapsulated) flexible Cu(In,Ga)Se_2 thin film photovoltaic devices (on polyimide foil substrate with Mo back electrode, CdS buffer layer and Al-doped zinc oxide front electrode) with 15, 25, 30, 50, 60 and 75 nm AlO_x layers (referred to as "CIGS" in the text and figures), and iii) six 15×15 cm^2 polyethylene terephthalate (PET) foil samples with 15, 25, 30, 50, 60 and 75 nm AlO_x layers. It should be noted that these thicknesses should be taken only as nominal deposition values. The AlO_x layers were deposited using trimethylaluminum (TMA) and water as precursors for aluminium and oxygen respectively. Layers were deposited at 100ºC, at 30 rpm, with 50 sccm TMA/950 sccm dilution and 750sccm H_2O at 50ºC/750 sccm dilution. The coated area had a donut shape (see **Figure 2a-c**) with slight thickness variations along the radial direction (decreasing from the centre to the edges) which allowed to test the sensitivity of the proposed methodology. For the Si and CIGS samples, the normal reflectance measurements were carried out in a mapping configuration (30×30 measuring points grid, approximately) covering the whole area of the samples (see **Figure 2d**). In the case of the PET samples, a special low reflectance (<5 % in the 300 – 700 nm range) holder had to be employed due to the high transparency of this material to the excitation wavelengths used for the analysis. In addition, the use of such holder prevented the use of the XY crane for the acquisition of large area mappings and the measurements were performed point-by-point, manually (15 points per sample).

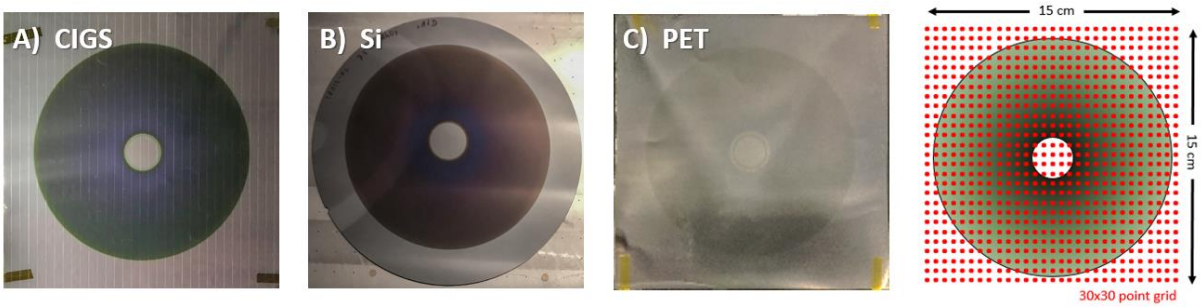

Figure 2. Picture of a) the CIGS-device, b) Si, and c) PET samples coated with a 75 nm AlO_x layer. The last is the approximate schematic of the samples and measuring points. Inner and outer radius of the deposition area are 1.2 cm and 7.6 cm respectively.

Additional measurements were carried out on the Si-based samples along the radial direction (9 points per sample) by means of ellipsometry (Horiba Jobin Yvon, Uvisel) to corroborate that the signal obtained from the surface of the substrate material varied as a consequence of the change of the optical properties of AlO_x with layer thickness. The measurements were made with a 70º angle of incidence.

Methodology

In order to quantify the differences in the normal reflectance spectra and translate them into thickness data, the following control parameter (q_t) was defined:

$$q_t = \sum_x \left| A_s(x) - A_{ref}(x) \right| \qquad (1)$$

where $A_s(x)$ is the integrated intensity of the normal reflectance spectra of the AlO_x layer in a selected spectral range x (400 – 900 nm in the case of the halogen lamp and 600 – 700 for the 660 nm LED) for a specific measuring point, and $A_{ref}(x)$ is the average integrated intensity in the same range of all the measuring points corresponding to the uncoated base (substrate). The use of q_t reduces the impact of potential sample-to-sample fluctuations in the normal reflectance spectra as a consequence of changes in the reflectivity of the base material (substrate) not related to the AlO_x layers. In this way, the use of this parameter allows improving the accuracy of the AlO_x thickness evaluation.

In order to provide a useful methodology for the thickness quantification, the q_t parameter was calculated for each measuring point and, then, all the q_t values obtained were averaged for each sample and plotted versus the nominal deposition thickness for each type of substrate/AlO_x sample. Through the fitting of such data, calibration curves were subsequently calculated to show the potential of the proposed methodology for predicting the thickness of an AlO_x layer from normal reflectance measurements.

Alternatively, a machine learning driven methodology based on the combination of principal component analysis (PCA) and linear discriminant analysis (LDA) algorithms was employed to quantify the normal reflectance spectra and translate them into thickness data. PCA and LDA are both dimension-reduction algorithms, and their combination was selected due to its wide-spread use for spectral data analysis in different methods and fields of application[32–37]. The goal of this algorithm is to learn to classify data into distinct groups defined by the user, and make predictions on new input data. In order to test and implement the machine learning based PCA-LDA algorithm the Python programing environment[38] with the Scikit-Learn library[39] was used. All the experimental data were randomly divided in 70% for training and 30% for testing and the input features were the same as those used to calculate the q_t parameter using equation (1). In the case of the in-sample analysis, the data points were divided in 5 groups corresponding to rings in the sample with rings 1 and 5 representing the outer and inner extremes, respectively (see **Figure S1**). To evaluate the performance of the algorithm, training and test scores are used. These values are calculated as the number of correctly classified points divided by the total amount, thus these values range from 0 to 1, being 0 no correct classifications at all and 1 when all points are correctly classified. The training scores were above 0.8 for the halogen lamp and above 0.6 for the LED light source (see **Figure 7** and **Figure 8**).

3. Results

3.1. Initial validation: Si/AlO_x samples

Before employing normal reflectance, preliminary ellipsometry measurements were carried out on Si/AlO_x samples with three different nominal layer thicknesses (25, 50 and 75 nm) and slight in-sample radial thickness gradient (see experimental section for further details) in order to corroborate that the optical properties of the samples change with the thickness of the AlO_x layer. The results are shown in **Figure 3b**. It can be observed that the Ψ and Δ angles of the complex reflectance ratio present slight in-sample changes along the radial direction within the different points measured (see **Figure 3a**) and abrupt sample-to-sample differences as a consequence of the varying thicknesses. These changes consist mainly of a blue-shift of the spectra as the AlO_x layer thickness is reduced. It should be noted that these variations represent the change of the complex reflectance of the Si-air structure as a consequence of the presence of an intermediate AlO_x layer with varying thicknesses. Since the optical properties of a layered structure are strongly intertwined with and can be derived from its complex reflectance ratio (using an adequate model), it can be concluded that the variation of the latter indicates a change

in the optical properties of AlO_x. Further analysis of the ellipsometry measurements to determine which specific properties are modified when the thickness of the AlO_x layers is varied is beyond the scope of this work. However, taking into account that the deposition conditions were identical for the three Si/AlO_x samples, the observed thickness-induced blue-shift can be attributed to quantum confinement QC effects.[40-42] However, other effects different to QC that may be contributing to the changes observed in the ellipsometry measurements cannot be discarded. The results that will be presented throughout this work are based on the correlation of these slight changes of the optical properties of AlO_x with normal reflectance measurements.

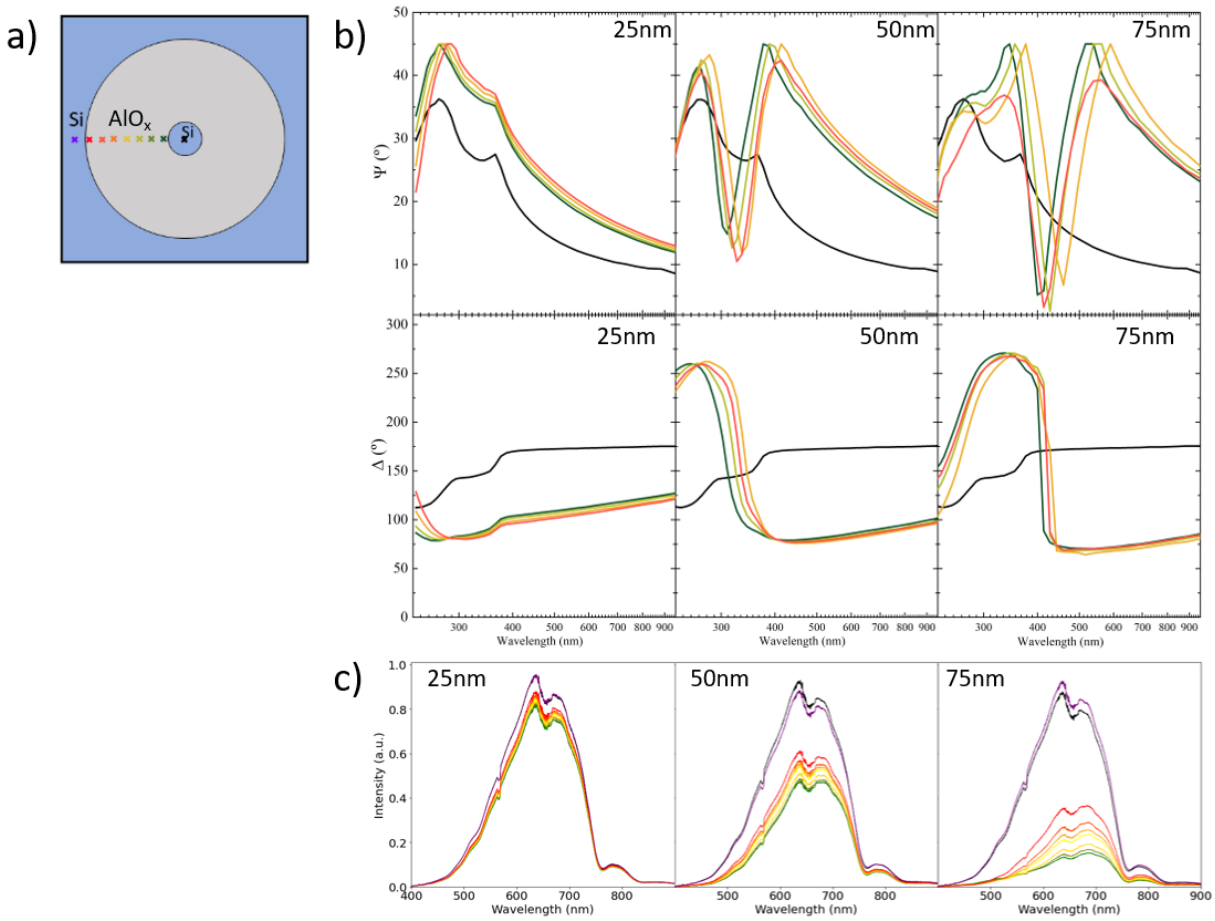

Figure 3. a) Colour code legend of the different measuring points. b) Complex reflectance ratio angles of the Si/AlO_x samples measured by ellipsometry in different positions along the radial direction. c) Raw normal reflectance spectra of the Si/AlO_x samples measured in similar positions.

In this way, the Si/AlO_x samples were subsequently measured in similar positions along the radial direction with the normal reflectance system described in the experimental section (see **Figure 1**) in order to make an initial validation of the technique to detect the small variations observed by ellipsometry. **Figure 3c** shows the raw normal reflectance data acquired on the Si/AlO_x samples. A similar shape can be observed for the spectra measured at different points along the radial direction of each sample with a broad band having the maximum position in

the 620 – 720 nm region, approximately. However, the intensity of this band is observed to vary from the centre (lower) to the edge (higher) of the sample in consonance with the thickness gradient of the deposited layers. The maximum intensity is reached for the bare uncoated Si substrate. On the other hand, clear sample-to-sample differences can be spotted not only as abrupt differences in the intensity of the reflectance spectra (with higher thickness leading the lower intensity), but also as a different shape of the reflectance band (with a faster decrease of the short wavelength part of the band as layer thickness increases). In addition, a higher in-sample variability is found as the nominal thickness of the deposited AlO_x layer increases. All these variations correlate well with those observed in the ellipsometry measurements (**Figure 3b**) and indicate that normal reflectance is sensitive both to AlO_x thickness variations in the order of tens of nm (sample-to-sample) but also to the slight nanometric variations (expected to be well below 10 nm) found within the layers.

Once that the sensitivity of the normal reflectance technique was proved to be high enough to detect small thickness variations, the proposed methodology was applied to the same Si samples coated with 25, 50 and 75 nm AlO_x layers but carrying out a mapping analysis covering the full surface of the sample (**Figure 4a**). The raw data (**Figure 4a**, left) show three different groups of spectra that have been highlighted with different colours in the figure. The groups with the highest (purple) and lowest (grey) intensities correspond to the Si substrate and to the measuring table, respectively. The last group (green-yellow gradient) encompasses all the AlO_x-coated points. As expected, the AlO_x spectra have the same characteristics as those shown in **Figure 3**, i.e. similar shape, gradual in-sample variations and more abrupt sample-to-sample differences with changes in the reflectance band intensity and shape, with higher variability in the thicker samples. In order to quantify the differences in the normal reflectance spectra and translate them into thickness data with high sensitivity, the q_t parameter was calculated for each point measured in every sample using equation (1). The obtained values are represented in the form of mappings in **Figure 4a** (right) where the bare Si, measuring table and donut-shaped AlO_x areas can be clearly distinguished. Furthermore, differences in q_t can be observed in the radial direction confirming the sensitivity of the technique to slight thickness variations below 10 nm. On the other hand, the mappings further confirm that in-sample thickness variability increases with the nominal thickness of the deposited AlO_x layer, with distribution limits for the q_t parameter roughly ranging from 50 – 100, 250 – 350, and 400 – 550 for the 25 nm, 50 nm and 75 nm samples, respectively. This indicates that the developed methodology can also be employed for high-resolution large area homogeneity control of deposited AlO_x layers.

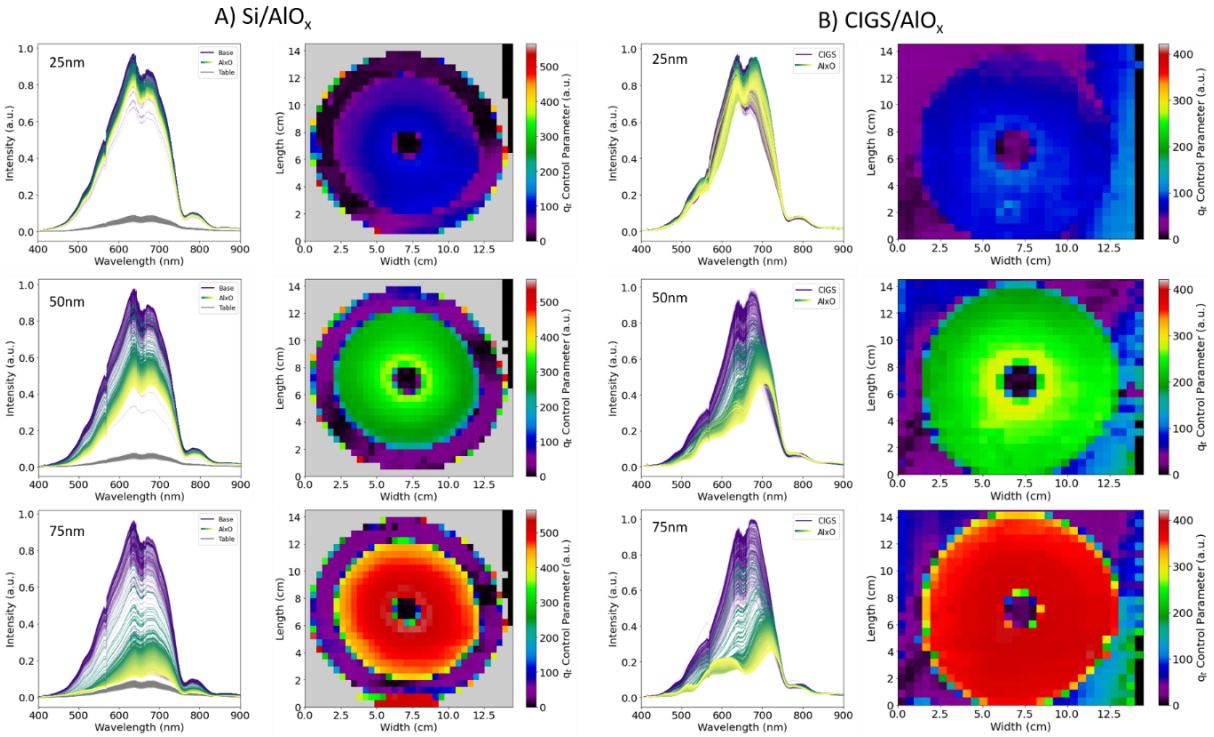

Figure 4. Raw reflectance spectra (left) and mappings of the calculated q_t parameter (right) for Si/AlO_x (a) and $CIGS/AlO_x$ (b) samples.

The data presented in **Figure 4a** were employed to calculate the average q_t in the donut-shaped AlO_x-covered areas. By plotting the average q_t versus the nominal thickness of the AlO_x layers, a calibration curve is obtained for correlating the reflectance data with the thickness of the AlO_x layers (**Figure 5a**). It can be observed that there appears to exist a quadratic relationship between the nominal thickness of the AlO_x layers and the q_t parameter. As such, these data demonstrate that normal reflectance offers a feasible and precise method for thickness assessment of AlO_x layers deposited on monocrystalline Si substrate.

3.2. Application of normal reflectance to AlO_x thickness estimation on CIGS and PET

Once that the proposed methodology was demonstrated for Si-based samples, it was applied to AlO_x layers (15, 25, 30, 50, 60 and 75 nm) deposited on relevant substrates regarding the encapsulation of thin film flexible PV devices: CIGS and PET.

In the case of the CIGS modules, a similar mapping to that described for the Si samples was performed. Three representative cases (25, 50 and 75 nm) are shown in **Figure 4b** while the complete results for all the different samples can be consulted in **Figure S2**. The raw spectra shown in the figures reveal a high degree of similarity to those obtained on Si samples with a broad band having the maximum position in the 620 – 720 nm region and with similar in-sample and sample-to-sample variability characteristics. However, a higher variability of the

reflectance signal arising from the base (CIGS substrate) is detected for thicknesses ≥ 50 nm, as well as a lower deviation for the thin AlO_x coatings ≤ 30 nm. This is detected despite the fact that for low AlO_x thickness values (≤ 30 nm), the intensity and shape of the spectra from the base and the AlO_x-covered areas present similar values. However, the q_t mappings show that the use of this parameter allows overcoming this issue and distinguishing the bare substrates from the donut-shaped AlO_x-covered areas, showing to be sensitive to even the small in-sample AlO_x thickness changes. The strong variations detected in the signal of the base material are related to local inhomogeneities of the CIGS absorber and/or CdS buffer layers of the devices, which are the main layers that reflect the excitation light employed (400 – 900 nm). The possibilities to overcome this obstacle will be discussed later on.

In the case of PET, the need of using a special low-reflectance holder prevented carrying out large area mappings. The spectra acquired are shown in **Figure S3**. Again, the spectra present similar characteristics as those of Si and CIGS samples. However, due to the low reflectivity of the base material (PET), almost no shape changes of the reflection band are detected which indicates that the sensitivity of the proposed methodology is lower for this material. Despite the lower sensitivity, the changes of the band intensity are marked enough to allow detecting differences between the different samples.

The average q_t and calibration curves obtained for AlO_x deposited on CIGS and PET are shown in **Figure 5b** and **Figure 5c**, respectively. These data demonstrate that normal reflectance can also be employed for determining the thickness of AlO_x encapsulation barrier layers deposited on multi-stack CIGS and rough PET substrates with high accuracy.

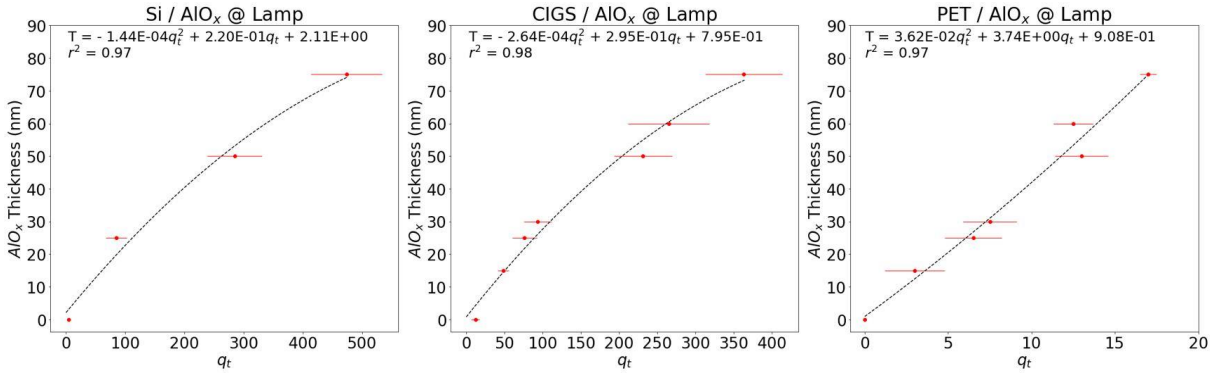

Figure 5. Average q_t (red dots) and fitted calibration curves (dashed curves) obtained for AlO_x deposited on Si (a), CIGS (b) and PET (c). The error bars correspond to the standard deviation (σ) of the different measured points.

3.3. Implementation of machine learning algorithms: CIGS test case

Although the use of the q_t control parameter and calibration curves is a perfectly suitable methodology for obtaining precise thickness measurements as demonstrated above, the amount of data generated in the large area mapping measurements carried out in this work provides an ideal test environment for the implementation of more advanced analysis techniques based on machine learning algorithms that could be suitable for analysis in industrial applications. As a proof of concept, a machine learning algorithm based on PCA-LDA (see more details in the experimental section) was applied to the experimental data obtained in the present study for the CIGS samples. These samples were selected as a the most relevant case for the present study since large area mappings were performed onto them and they present a rough surface that makes thickness estimation challenging by other techniques. Both the capacity to detect sample-to-sample and in-sample variations were tested. The results are shown in **Figure 6**.

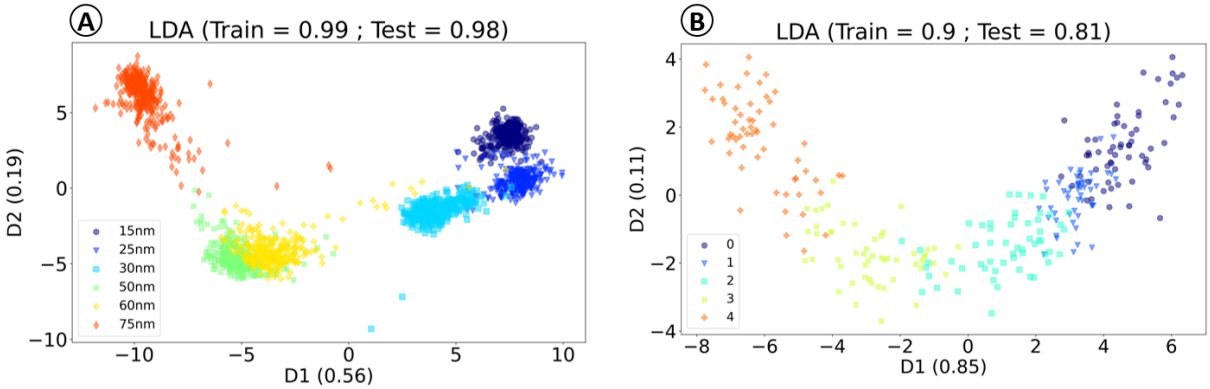

Figure 6. PCA-LDA sample-to-sample (A) and in-sample (B) thickness classification results for CIGS samples. The in-sample variation analysis was performed on the 75 nm AlO_x sample with the data grouped by rings in the radial direction (see Figure S1).

Regarding the sample-to-sample analysis, it can be observed that the PCA-LDA algorithm enables a clear classification of the samples with different nominal thicknesses yielding a test score very close to 1 (**Figure 6a**). This is somehow remarkable taking into account that, as already mentioned, all the samples present a slight thickness radial gradient which inevitably produces a broadening in the classification groups complicating classification. For example, it is interesting to note that although some overlapping is clearly observed for the 50 and 60 nm samples, the algorithm is still capable of correctly classifying the points according to AlO_x nominal layer thickness.

As for the in-sample variability, the 75 nm AlO_x sample was analyzed by dividing the data points in groups corresponding to 5 rings in the sample with rings 1 and 5 representing the outer and inner extremes, respectively (see **Figure S1**). As shown in **Figure 6b**, the algorithm enables

to effectively classify the points by the different thickness ring to which they belong proving, again, the high sensitivity of the proposed normal reflectance methodology to thickness variations < 10 nm. Although some overlapping can be observed between the different groups, this is mostly due to the thickness grading existent within the rings.

These results prove the feasibility of employing a machine learning driven analysis coupled to the proposed normal reflectance approach as a powerful alternative to that based on calibration curves for process monitoring in an industrial environment enabling measuring nanocoating thicknesses with sensitivities < 10 nm. Furthermore, it should be taken into account that the amount of data employed for the analysis (~2640 spectra) is far from being considered "big data" and, as such, that this methodology can be further improved for a more precise classification using a higher number of training inputs.

4. Discussion: Implementing normal reflectance for industrial in-line process monitoring

Although normal reflectance has previously been employed for thin film thickness evaluation at research[43-35] and process monitoring[27] levels, this was done through the use of complex and expensive systems, long acquisition times, models based on previous knowledge on the optical properties of the material and/or for thicknesses larger than those used in the applications described here. In this way, the results presented in this work, represent a laboratory proof-of-concept of a completely different and innovative approach that demonstrate the feasibility of directly employing normal reflectance data for a precise and fast determination of the thickness of nanometric AlO_x layers deposited on Si, CIGS and PET employing a simple and inexpensive system. In this regard, it should be noted that the main novelty of this work lies in the fact that the methodology proposed does not require to understand the physical meaning of the differences observed in the normal reflectance spectra, but only to be able to detect these differences and correlate them to the thickness of the AlO_x nanometric layers. However, the main focus of this methodology is its implementation in industrial environments, especially for process monitoring of AlO_x barrier layers deposited by S-ALD in RtR configuration. In this context, several aspects must be considered in order to make the normal reflectance methodology more industrially-friendly.

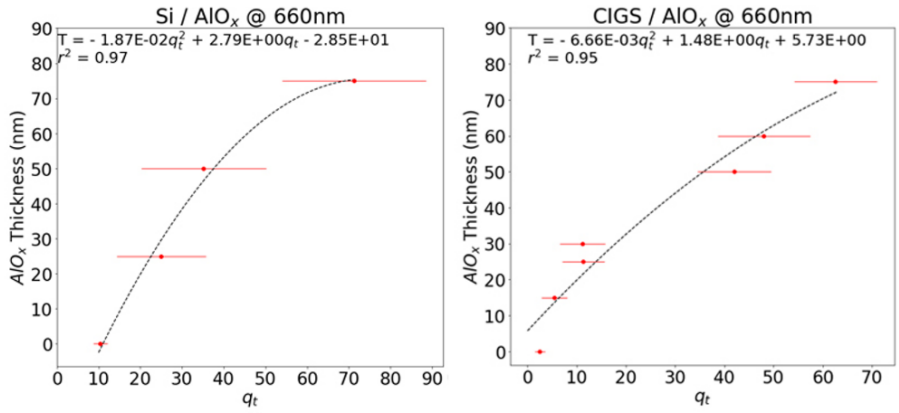

Figure 7. Example of reflectance calibration curves obtained with a 660 nm LED source for Si/AlO_x (a) and $CIGS/AlO_x$ (b) samples.

The first aspect that should be considered, is the substitution of the excitation light source based on a standard halogen lamp by a more stable, maintenance-free, versatile and low-cost one. In this regard, LED-based light sources are more appropriate for the industry. The feasibility of employing a monochromatic LED light source (660 nm) was tested for the Si and CIGS samples presented above. Taking a look at the calibration curves obtained under LED illumination (**Figure 7**), it can be seen that a very high dispersion is obtained for the q_t parameter in the case of the Si base. As for CIGS, except for the 25 and 30 nm samples which seem undistinguishable due to their similar q_t values, the results show that the LED excitation source works in a fairly similar fashion as the halogen lamp.

Additionally, the same machine learning-based analysis performed for the halogen lamp measurements in the CIGS samples was applied to the spectral data acquired with the LED light source (**Figure 8**). Regarding sample-to-sample analysis (**Figure 8a**), the test score for point classification is significantly lower than in the case of the halogen lamp. It can be observed that this is due to the fact that the 15-30 nm and 50-60 nm samples present a high overlapping leading to misclassification of the groups. This is in accordance with the results obtained with the calibration curve presented in **Figure 7** for these samples. Similarly, the in-sample classification (**Figure 8b**) also presents a lower score and higher overlapping than in the case of the halogen lamp.

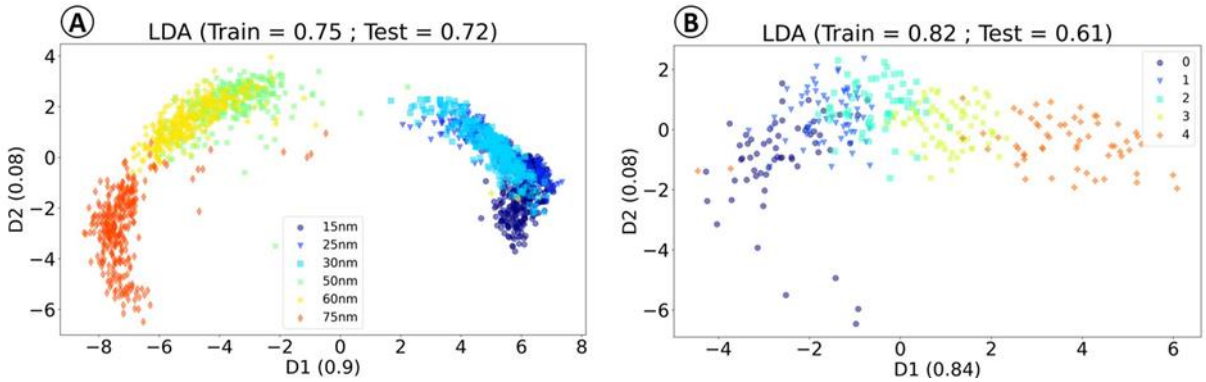

Figure 8. PCA-LDA sample-to-sample (A) and in-sample (B) thickness classification results for CIGS samples measured with an LED light source. The in-sample variation analysis was performed on the 75 nm of AlO_x sample with the data grouped by rings in the radial direction (see Figure S1).

All these dispersion/overlapping issues, though, can be resolved by tailoring the LED excitation employed to the characteristics of the sample to maximize the reflectance signal. Furthermore, the use of several multiplexed LED sources with different wavelengths would open the way to further optimization of the signal acquisition. Either way, the results shown in **Figure 7** and **Figure 8** indicate that the methodologies presented in this work are versatile in terms of the possibility of employing different illumination sources tailored to the characteristics of the material to be analyzed, enabling the optimization of the system in a simple way.

Another critical aspect that should be taken into account for industrial implementation of a normal reflection-based monitoring tool is the methodology employed for calculating q_t. In this work, $A_{ref}(x)$ was defined in Equation (1) as the average integrated intensity of all the spectra corresponding to the base material (see experimental section for further details). It was defined in such manner because the samples were analyzed only after AlO_x deposition. Although the use of this parameter has been shown to be critical for obtaining measurements with high precision, the high variability of the reflectance signal throughout the different points of the base material is one of the reasons why the measurements present a high dispersion hindering the differentiation of AlO_x layers with low thicknesses from the bare substrate. Nevertheless, in an industrial process monitoring environment, two optical probes located before and after the AlO_x deposition process, and synchronized to measure in the exact same position would allow calculating $A_{ref}(x)$ for each measuring point (instead of using an average value) minimizing the signal fluctuations related to the inhomogeneities of the base material and improving the accuracy and reliability of the methodology. **Figure 9** schematically depicts the design of such a system. On the other hand, it should be taken into account, that besides the dispersion introduced by the inhomogeneity of the base materials, the samples analyzed in this

work had an intentional AlO_x thickness gradient along the radial direction which has introduced additional dispersion. This has also importantly contributed to the difficulties observed to distinguish the AlO_x deposited areas from the bare substrate for low layer thicknesses. However, the results presented throughout the work have shown that the methodology employed is sensitive to these slight thickness changes of a few nm. As such, if $A_{ref}(x)$ and q_t are estimated individually for each measuring point, the resolution of the measurements would clearly be well below 10 nm allowing to precisely estimate the thickness of the AlO_x layers and carrying out high-resolution homogeneity control of deposited AlO_x layers in large areas. Moreover, changing the measuring spot from µm to cm size would allow performing both micro and macro homogeneity evaluations of the thickness of the layers.

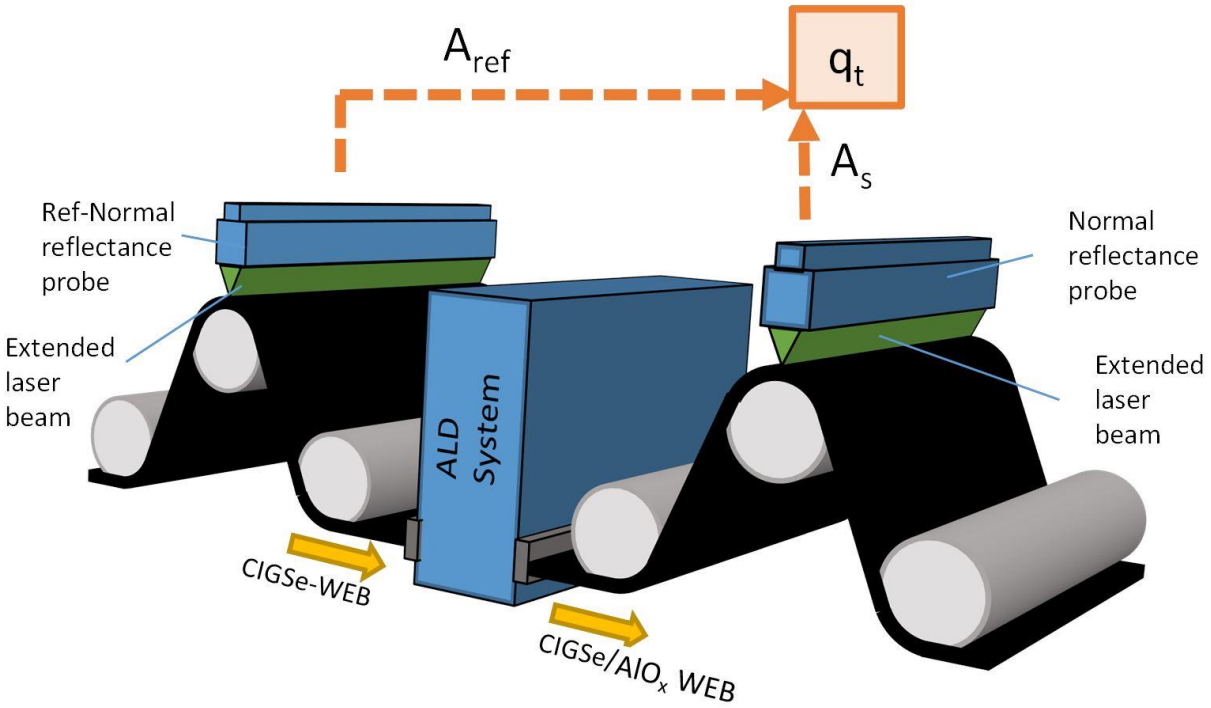

Figure 9. Integration of a normal reflectance-based process monitoring tool in a RtR S-ALD AlO_x deposition process.

Finally, as demonstrated in this work for low amount of spectra, in an industrial environment where an extremely large amount of data are expected to be obtained continuously, the implementation of machine learning algorithms for data analysis would also represent an advantageous strategy for improving the precision of the measurements thanks to its higher resilience to both sample and instrumental related fluctuations, fast training and classification, continuous self-improvement, and versatility in comparison to the use of calibration curves.

5. Conclusions

In this work, a novel solution has been proposed and demonstrated for determining the thickness of AlO_x nanometric coatings using normal reflectance measurements: a non-destructive, fast, precise, low-cost and scalable characterization method that can be implemented both in research and industrial process monitoring environments. The approach is based on detecting variations in the normal reflectance signal of a base/AlO_x/air sample originated as a consequence of the varying nanolayer thickness. The viability of the proposed solution for the analysis of AlO_x layer thickness in PV devices has been demonstrated employing a self-designed normal reflectance system and analyzing AlO_x nanolayers deposited on Si, CIGS and PET substrates. Large area mappings covering the full surface of the samples have been performed and methodologies based both on control parameter-based calibration curves and machine learning algorithms have been developed to relate the reflectance signal to the thickness of the AlO_x layers for each type of sample. These methodologies have been proven to be sensitive to thickness variations below 10 nm and have been demonstrated to be reliable for monitoring the AlO_x layers thickness in large area industrial environments with high resolution. Additionally, the limitations of the technique as well as the most critical aspects that should be regarded to implement a normal reflectance-based tool for industrial process monitoring have been discussed. As such, this work paves the way for developing a novel characterization technology that has direct application for monitoring industrial AlO_x-based encapsulation processes for flexible thin film PV modules but that can also be extended to many other industrial applications that require a precise and simple way of evaluating the thickness of nanocoatings.

Supporting Information

Supporting Information is available from the Wiley Online Library or from the author.

Acknowledgements

This work has been partially funded by the European Union H2020 Framework Program (H2020-LCE-2017-RES-IA) under Grant Agreement no. 792245 (SuperPV). The authors from IREC and the University of Barcelona are grateful to Solar-ERA.NET DURACIS project (Spanish subproject funded by MICIIN nr. PCIN-2017-041), are supported by the European Regional Development Funds (ERDF, FEDER Programa Competitivitat de Catalunya 2007–2013), and belong to the SEMS (Solar Energy Materials and Systems) Consolidated Research

Group of the “Generalitat de Catalunya” (Ref. 2017SGR 862). M.G. acknowledges the financial support from ACCIÓ-Generalitat de Catalunya within the TECNIOspring Plus fellowship (TECSPR18-1-0048).

References

(1) Becerril-Romero, I. Alternative Substrates for Sustainable and Earth-Abundant Thin Film Photovoltaics. PhD Thesis, Universitat de Barcelona, Barcelona, 2019.

(2) Dhere, N. G. Flexible Packaging for PV Modules; Dhere, N. G., Ed.; San Diego, CA, 2008; p 70480R. https://doi.org/10.1117/12.795718.

(3) Leterrier, Y. Durability of Nanosized Oxygen-Barrier Coatings on Polymers. *Progress in Materials Science* **2003**, *48* (1), 1–55. https://doi.org/10.1016/S0079-6425(02)00002-6.

(4) Hirvikorpi, T.; Laine, R.; Vähä-Nissi, M.; Kilpi, V.; Salo, E.; Li, W. M.; Lindfors, S.; Vartiainen, J.; Kenttä, E.; Nikkola, J.; Harlin, A.; Kostamo, J. Barrier Properties of Plastic Films Coated with an Al2O 3 Layer by Roll-to-Toll Atomic Layer Deposition. *Thin Solid Films* **2014**, *550*, 164–169. https://doi.org/10.1016/j.tsf.2013.10.148.

(5) Carcia, P. F.; McLean, R. S.; Hegedus, S. Encapsulation of Cu(InGa)Se_2 Solar Cell with Al_2O_3 Thin-Film Moisture Barrier Grown by Atomic Layer Deposition. *Solar Energy Materials and Solar Cells* **2010**, *94* (12), 2375–2378. https://doi.org/10.1016/j.solmat.2010.08.021.

(6) Zhang, Y.; Bertrand, J. A.; Yang, R.; George, S. M.; Lee, Y. C. Electroplating to Visualize Defects in Al_2O_3 Thin Films Grown Using Atomic Layer Deposition. *Thin Solid Films* **2009**, *517* (11), 3269–3272. https://doi.org/10.1016/j.tsf.2008.12.052.

(7) Cooper, R.; Upadhyaya, H. P.; Minton, T. K.; Berman, M. R.; Du, X.; George, S. M. Protection of Polymer from Atomic-Oxygen Erosion Using Al_2O_3 Atomic Layer Deposition Coatings. *Thin Solid Films* **2008**, *516* (12), 4036–4039. https://doi.org/10.1016/j.tsf.2007.07.150.

(8) Groner, M. D.; George, S. M.; McLean, R. S.; Carcia, P. F. Gas Diffusion Barriers on Polymers Using Al_2O_3 Atomic Layer Deposition. *Appl. Phys. Lett.* **2006**, *88* (5), 051907. https://doi.org/10.1063/1.2168489.

(9) Carcia, P. F.; McLean, R. S.; Reilly, M. H.; Groner, M. D.; George, S. M. Ca Test of Al_2O_3 Gas Diffusion Barriers Grown by Atomic Layer Deposition on Polymers. *Appl. Phys. Lett.* **2006**, *89* (3), 031915. https://doi.org/10.1063/1.2221912.

(10) Poodt, P.; Cameron, D. C.; Dickey, E.; George, S. M.; Kuznetsov, V.; Parsons, G. N.; Roozeboom, F.; Sundaram, G.; Vermeer, A. Spatial Atomic Layer Deposition: A Route towards Further Industrialization of Atomic Layer Deposition. *Journal of Vacuum Science & Technology A: Vacuum, Surfaces, and Films* **2012**, *30* (1), 010802. https://doi.org/10.1116/1.3670745.

(11) Poodt, P.; Knaapen, R.; Illiberi, A.; Roozeboom, F.; van Asten, A. Low Temperature and Roll-to-Roll Spatial Atomic Layer Deposition for Flexible Electronics. *J. Vac. Sci. Technol. A* **2012**, *30* (1), 6.

(12) Li, J.; Wang, Y.; Wan, F.; An, M.; Li, M.; Wang, L.; Zhang, X.; Liu, Y. Passivation via Atomic Layer Deposition Al2O3 for the Performance Enhancement of Quantum Dot Photovoltaics. *Solar Energy Materials and Solar Cells* **2020**, *209* (January), 110479. https://doi.org/10.1016/j.solmat.2020.110479.

(13) Fan, P.; Sun, Z.; Wilkes, G. C.; Gupta, M. C. Low-Temperature Laser Generated Ultrathin Aluminum Oxide Layers for Effective c-Si Surface Passivation. *Applied Surface Science* **2019**, *480* (August 2018), 35–42. https://doi.org/10.1016/j.apsusc.2019.02.023.

(14) Ojeda-Durán, E.; Monfil-Leyva, K.; Andrade-Arvizu, J.; Becerril-Romero, I.; Sánchez, Y.; Fonoll-Rubio, R.; Guc, M.; Jehl, Z.; Luna-López, J. A.; Muñoz-Zurita, A. L.; Hernández-de la Luz, J. A. D.; Izquierdo-Roca, V.; Placidi, M.; Saucedo, E. CZTS Solar Cells and the Possibility of Increasing VOC Using Evaporated Al2O3 at the CZTS/CdS Interface. *Solar Energy* **2020**, *198* (January), 696–703. https://doi.org/10.1016/j.solener.2020.02.009.

(15) Choi, S.; Kamikawa, Y.; Nishinaga, J.; Yamada, A.; Shibata, H.; Niki, S. Lithographic Fabrication of Point Contact with Al2O3 Rear-Surface-Passivated and Ultra-Thin Cu(In,Ga)Se2 Solar Cells. *Thin Solid Films* **2018**, *665*, 91–95. https://doi.org/10.1016/j.tsf.2018.08.044.

(16) Lim, J. W. M.; Chan, C. S.; Xu, L.; Ong, T. M.; Huang, S. Y.; Wei, D. Y.; Guo, Y. N.; Xu, S. High Quality Hydrogenated Amorphous Silicon Thin Films with Enhanced Growth Rates for Surface Passivation in an Al2O3 Based ICP Reactor. *Procedia Engineering* **2016**, *139*, 56–63. https://doi.org/10.1016/j.proeng.2015.09.216.

(17) Hwang, B. U.; Kim, D. Il; Cho, S. W.; Yun, M. G.; Kim, H. J.; Kim, Y. J.; Cho, H. K.; Lee, N. E. Role of Ultrathin Al2O3 Layer in Organic/Inorganic Hybrid Gate Dielectrics for Flexibility Improvement of InGaZnO Thin Film Transistors. *Organic Electronics* **2014**, *15* (7), 1458–1464. https://doi.org/10.1016/j.orgel.2014.04.003.

(18) Vermang, B.; Fjallström, V.; Gao, X.; Edoff, M. Improved Rear Surface Passivation of Cu(In,Ga)Se2 Solar Cells: A Combination of an Al2O3 Rear Surface Passivation Layer and Nanosized Local Rear Point Contacts. *IEEE Journal of Photovoltaics* **2014**, *4* (1), 486–492. https://doi.org/10.1109/JPHOTOV.2013.2287769.

(19) Gunter, P. L. J.; Niemantsverdriet, J. W. Thickness Determination of Uniform Overlayers on Rough Substrates: A Comparison of Calculations for Al_2O_3/Al to X-ray Photoelectron Spectroscopy and Atomic Force Microscopy Experiments on Technical Aluminum Foils. *Journal of Vacuum Science & Technology A: Vacuum, Surfaces, and Films* **1995**, *13* (3), 1290–1292. https://doi.org/10.1116/1.579552.

(20) Wang, X.; Xiang, J.; Wang, W.; Zhao, C.; Zhang, J. Dependence of Electrostatic Potential Distribution of Al_2O_3/Ge Structure on Al_2O_3 Thickness. *Surface Science* **2016**, *651*, 94–99. https://doi.org/10.1016/j.susc.2016.04.001.

(21) Suárez-Campos, G.; Cabrera-German, D.; Castelo-González, A. O.; Avila-Avendano, C.; Fuentes Ríos, J. L.; Quevedo-López, M. A.; Aceves, R.; Hu, H.; Sotelo-Lerma, M. Characterization of Aluminum Oxide Thin Films Obtained by Chemical Solution Deposition and Annealing for Metal–Insulator–Metal Dielectric Capacitor Applications. *Applied Surface Science* **2020**, *513*. https://doi.org/10.1016/j.apsusc.2020.145879.

(22) Hyde, G. K.; McCullen, S. D.; Jeon, S.; Stewart, S. M.; Jeon, H.; Loboa, E. G.; Parsons, G. N. Atomic Layer Deposition and Biocompatibility of Titanium Nitride Nano-Coatings on Cellulose Fiber Substrates. *Biomed. Mater.* **2009**, *4* (2), 025001. https://doi.org/10.1088/1748-6041/4/2/025001.

(23) Martinez, G.; Shutthanandan, V.; Thevuthasan, S.; Chessa, J. F.; Ramana, C. V. Effect of Thickness on the Structure, Composition and Properties of Titanium Nitride Nano-Coatings. *Ceramics International* **2014**, *40* (4), 5757–5764. https://doi.org/10.1016/j.ceramint.2013.11.014.

(24) Erlat, A. G.; Henry, B. M.; Grovenor, C. R. M.; Briggs, A. G. D.; Chater, R. J.; Tsukahara, Y. Mechanism of Water Vapor Transport through PET/AlOxNy Gas Barrier Films. *Journal of Physical Chemistry B* **2004**, *108* (3), 883–890. https://doi.org/10.1021/jp036244y.

(25) Kobayashi, N. P.; Donley, C. L.; Wang, S. Y.; Williams, R. S. Atomic Layer Deposition of Aluminum Oxide on Hydrophobic and Hydrophilic Surfaces. *Journal of Crystal Growth* **2007**, *299* (1), 218–222. https://doi.org/10.1016/j.jcrysgro.2006.11.224.

(26) Srinivasan, K.; Kottantharayil, A. Aluminium Oxide Thin Film Deposited by Spray Coating for P-Type Silicon Surface Passivation. *Solar Energy Materials and Solar Cells* **2019**, *197* (March), 93–98. https://doi.org/10.1016/j.solmat.2019.03.048.

(27) Sakalak, H.; Yılmaz, K.; Gürsoy, M.; Karaman, M. Roll-to Roll Initiated Chemical Vapor Deposition of Super Hydrophobic Thin Films on Large-Scale Flexible Substrates. *Chemical Engineering Science* **2020**, 8.

(28) González-Ramírez, J. E.; Fuentes, J.; Hernández, L. C.; Hernández, L. Evaluation of the Thickness in Nanolayers Using the Transfer Matrix Method for Modeling the Spectral Reflectivity. *Research Letters in Physics* **2009**, *2009*, 1–4. https://doi.org/10.1155/2009/594175.

(29) Bermudez, V.; Perez-Rodriguez, A. Understanding the Cell-to-Module Efficiency Gap in Cu(In,Ga)(S,Se)2 Photovoltaics Scale-Up. *Nature Energy* **2018**, *3* (6), 466–475. https://doi.org/10.1038/s41560-018-0177-1.

(30) Lin, T.; Wan, M.; Xu, J.; Xu, L.; Chen, K. J. Size-Dependent Optical Properties of SnO 2 Nanoparticles Prepared by Soft Chemical Technique. *Journal of Nanoscience and Nanotechnology* **2010**, *10* (7), 4357–4362. https://doi.org/10.1166/jnn.2010.2203.

(31) Illiberi, A.; Frijters, C.; Ruth, M.; Bremaud, D.; Poodt, P.; Roozeboom, F.; Jan, P. Atmospheric Spatial Atomic Layer Deposition of ZnOS Buffer Layers for Flexible Cu(In,Ga)Se_2 Solar Cells. *J. Vac. Sci. Technol. A* **2018**, *36* (5), 8.

(32) Ralbovsky, N. M.; Lednev, I. K. Raman Spectroscopy and Chemometrics: A Potential Universal Method for Diagnosing Cancer. *Spectrochimica Acta Part A: Molecular and Biomolecular Spectroscopy* **2019**, *219*, 463–487. https://doi.org/10.1016/j.saa.2019.04.067.

(33) Chauhan, R.; Kumar, R.; Kumar, V.; Sharma, K.; Sharma, V. On the Discrimination of Soil Samplesby Derivative Diffuse Reflectance UV-Vis-NIR Spectroscopy and Chemometric Methods. *Forensic Science International* **2020**, 110655. https://doi.org/10.1016/j.forsciint.2020.110655.

(34) Guleken, Z.; Ünübol, B.; Bilici, R.; Sarıbal, D.; Toraman, S.; Gündüz, O.; Kuruca, S. E. Investigation of the Discrimination and Characterization of Blood Serum Structure in Patients with Opioid Use Disorder Using IR Spectroscopy and PCA-LDA Analysis. *Journal of Pharmaceutical and Biomedical Analysis* **2020**, *190*, 113553. https://doi.org/10.1016/j.jpba.2020.113553.

(35) Chophi, R.; Sharma, S.; Singh, R. Forensic Analysis of Red Lipsticks Using ATR-FTIR Spectroscopy and Chemometrics. *Forensic Chemistry* **2020**, *17*, 100209. https://doi.org/10.1016/j.forc.2019.100209.

(36) Visnevschi-Necrasov, T.; Barreira, J. C. M.; Cunha, S. C.; Pereira, G.; Nunes, E.; Oliveira, M. B. P. P. Phylogenetic Insights on the Isoflavone Profile Variations in Fabaceae Spp.: Assessment through PCA and LDA. *Food Research International* **2015**, *76*, 51–57. https://doi.org/10.1016/j.foodres.2014.11.032.

(37) Wang, Y.; Zhu, J.; Chen, X. Autofluorescence Spectroscopy of Blood Plasma with Multivariate Analysis Methods for the Diagnosis of Pulmonary Tuberculosis. *Optik* **2020**, *224*, 165446. https://doi.org/10.1016/j.ijleo.2020.165446.

(38) Python Software Foundation. Python Language Reference, version 3.9.0. Available at http://www.python.org.

(39) Pedregosa, F.; Varoquaux, G.; Gramfort, A.; Michel, V.; Thirion, B.; Grisel, O.; Blondel, M.; Prettenhofer, P.; Weiss, R.; Dubourg, V.; Vanderplas, J.; Passos, A.; Cournapeau, D.; Brucher, M.; Perrot, M.; Duchesnay, É. Scikit-Learn: Machine Learning in Python. *Journal of Machine Learning Research* **2011**, *12* (85), 2825–2830.

(40) Alonso, M. I.; Marcus, I. C.; Garriga, M.; Goñi, A. R.; Jedrzejewski, J.; Balberg, I. Evidence of Quantum Confinement Effects on Interband Optical Transitions in Si Nanocrystals. *Phys. Rev. B* **2010**, *82* (4), 045302. https://doi.org/10.1103/PhysRevB.82.045302.

(41) Fairbrother, A.; Izquierdo-Roca, V.; Fontané, X.; Ibáñez, M.; Cabot, A.; Saucedo, E.; Pérez-Rodríguez, A. ZnS Grain Size Effects on Near-Resonant Raman Scattering: Optical Non-Destructive Grain Size Estimation. *CrystEngComm* **2014**, *16* (20), 4120. https://doi.org/10.1039/c3ce42578a.

(42) Becerril-Romero, I.; Sylla, D.; Placidi, M.; Sánchez, Y.; Andrade-Arvizu, J.; Izquierdo-Roca, V.; Guc, M.; Pérez-Rodríguez, A.; Grini, S.; Vines, L.; Pusay, B.; Almache R.; Puigdollers, J.; Pistor, P.; Saucedo, E.; Espíndola-Rodríguez, M. Transition-Metal

Oxides for Kesterite Solar Cells Developed on Transparent Substrates. *ACS Appl. Mater. Interfaces* **2020**, 12 (30), 33656–33669

https://doi-org /10.1021/acsami.0c06992.

(43) Harbecke, B.; Heinz, B.; Grosse, P.; Optical properties of thin films and the Berreman effect. *Appl. Phys. A* **1985**, 38, 263–267.

https://doi.org/10.1007/BF00616061.

(44) Ventura, S. D.; Birgin, E. G.; Martínez, J. M.; Chambouleyron, I. Optimization techniques for the estimation of the thickness and the optical parameters of thin films using reflectance data. *J. Appl. Phys* **2005**, 97 (4), 043512. https://doi.org/10.1063/1.1849431.

(45) Ohlídal, M.; Ohlídal, I.; Franta, D.; Králík, T.; Jákl, M.; Eliáš, M. Optical characterization of thin films non-uniform in thickness by a multiple-wavelength reflectance method. *Surf. Interface Anal.* **2002**, 34, 660-663. https://doi-org/10.1002/sia.1382.